The merger history of clusters and its effect on the X-ray properties of the intracluster medium

David R. Rowley,* Peter A. Thomas and Scott T. Kay
Astronomy Centre, Department of Physics and Astronomy, University of Sussex, Brighton BN1 9QH

ABSTRACT

We investigate the growth over time of 20 massive (>3 keV) clusters in a hydrodynamical simulation of the Λ cold dark matter cosmology with radiative cooling. The clusters show a variety of formation histories: some accrete most of their mass in major mergers; others, more gradually. During major mergers, the long-term (temporally smoothed) luminosity increases such that the cluster moves approximately along the L_X–T_X relation; between times, it slowly decreases, tracking the drift of the L_X–T_X relation. We identify several different kinds of short-term luminosity and temperature fluctuations associated with major mergers including double-peaked mergers, in which the global intracluster medium merges first (L_X and T_X increase together) and then the cluster cores merge (L_X increases and T_X decreases). At both luminosity peaks, clusters tend to appear to be spherical and relaxed, which may lead to biases in high-redshift, flux-limited samples. There is no simple relationship between scatter in the L_X–T_X relation nor in the recent or overall merger activity or cluster formation time. The scatter in the L_X–M and T_X–M relations is reduced if properties are measured within R_{500} rather than $R_{\rm vir}$.

Key words: galaxies: clusters: general.

1 INTRODUCTION

Clusters of galaxies are the largest virialized structures in the Universe and mergers between them are among the most energetic events. This paper presents results from resimulations of 20 massive clusters to investigate the effects of the merger history on the X-ray properties of the intracluster medium (ICM).

In recent years high-quality observations of the ICM of distant clusters of galaxies have become available. This has enabled cosmological evolution studies to be carried out on clusters by looking at, for example, the high-redshift L_X–T_X relation (Fairley et al. 2000; Borgani et al. 2001; Holden et al. 2002; Novicki, Sornig & Henry 2002; Vikhlinin et al. 2002). This paper will look in detail at the merger history of clusters of galaxies and how this affects their X-ray properties. Previous observational studies of merging clusters of galaxies include Markevitch et al. (2002), Maughan et al. (2003) and Reiprich, Sarazin & Kempner (2003), and Allen, Schmidt & Fabian (2002) found evidence that the hottest cluster known (RX J1347.5-1145) is undergoing a merger. We find examples in our simulated clusters that mimic these observed clusters.

The merger rates of simulated cold dark matter (CDM) haloes were first investigated by Lacey & Cole (1994) and Navarro, Frenk & White (1995). The results were found to be in agreement with the analytical model of Lacey & Cole (1993). Wechsler et al. (2002) and Zhao et al. (2003) looked at the effects of mergers and accretion on the structure of individual CDM haloes and found that halo concentration tends to increase with increasing formation redshift.

To investigate the effects of mergers on the ICM, Pearce, Thomas & Couchman (1994) simulated the collision of pairs of relaxed cluster haloes and compared these with earlier dark matter only simulations (Pearce, Thomas & Couchman 1993). They found that the entropy structure of both the dark matter and the gas is relatively unchanged during the merger, although there is a small tendency to transfer energy from the former to the latter in the core of the system. The time evolution of the X-ray properties of merging clusters were investigated by Ritchie & Thomas (2002) in higher-resolution simulations that also included radiative cooling. They showed that the X-ray temperature and luminosity can temporarily increase by a large factor during a merger; the central entropy increase after the merger was found to be a strong function of subcluster mass and impact parameter.

The simulations described above started with isolated, relaxed clusters and investigated different impact parameters and mass ratios. However, real clusters in a cosmological environment are more complicated. They will have some amount of substructure, may be rotating and could collide with more than one subclump at a time. Therefore, to find out what kind of mergers clusters tend to undergo and the effect this has on the complex ICM, full cosmological simulations need to be carried out. A first step in this direction

was undertaken by Eke, Navarro & Frenk (1998). They undertook resimulations of individual clusters extracted from a dark matter simulation and showed that the evolution of bulk properties of clusters varied from cluster to cluster. The simulations that we describe in this paper are similar in spirit, but have more particles, include radiative cooling of the gas component, and have a much higher time resolution with which to follow the development of the X-ray properties.

We should also mention a couple of other recent studies. Randall, Sarazin & Ricker (2002) looked at the observational bias that can be induced by the temporary enhancements in luminosity and temperature in merging clusters on determinations of σ_8 and the number density of high-redshift clusters. Motl et al. (2004) undertook radiative simulations of a sample of two clusters and showed that the traditional model of smooth accretion on to clusters is inaccurate in that clusters accrete gas in subclumps which bring precooled gas direct to the core of a cluster. Our work supports both of these ideas.

The rest of this paper is organized as follows. In Section 2 the properties of the simulations and the resimulation technique will be described. Section 3 will investigate the mass, luminosity and temperature evolution of the resimulated clusters, with particular types of event being identified and examples of these looked at in detail. The link between scatter in the scaling relations and merger history or substructure will be investigated in Section 4. Finally, in Section 5, we summarize our results and compare the features seen in the simulations to observations.

2 THE SIMULATIONS

In a previous paper, Muanwong et al. (2002, hereafter MTKP02), X-ray scaling relations were presented for simulated catalogues containing over 400 groups and clusters. However, because of the volume simulated, only seven of these had virial temperatures in excess of 3 keV. This study simulates a further 20 such clusters by resimulating regions within a larger box, with the high-resolution regions having simulation parameters identical to that of the earlier run.

Three simulations were undertaken with parameters as shown in Table 1. The effective number of particles is the number of particles needed to fill the entire simulation volume at the highest resolution in the box. In the simulation HGAS there were equal numbers of gas and dark matter particles in the high-resolution regions. The mass resolution for HGAS refers to the sum of the two species.

2.1 The resimulation technique

We first generated a low-resolution run (LDM) with 160^3 dark matter particles. This was run to completion (from $z = 49$ to 0) and the 20 largest clusters identified using the technique described in MTKP02. All the particles within 2 virial radii of the cluster centres were identified. The locations of all these particles on the initial comoving grid (i.e. before the Zel'dovich approximation is applied) were noted and, along with the neighbouring grid points,

Table 1. Simulation parameters for the three runs: name, effective number of particles, particle mass in units of h^{-1} $M_{\odot}$, softening in units of h^{-1} kpc and particle species simulated.

Name	Particles	Mass	Soft.	Particle types
LDM	160^3	1.9×10^{11}	50	Dark matter
HDM	320^3	2.4×10^{10}	25	Dark matter
HGAS	2×320^3	2.4×10^{10}	25	Dark matter + gas

were flagged as requiring high resolution. Just under 4 per cent of the box was included in the high-resolution mask.

A second set of initial conditions was then generated on a 320^3 grid. The original waves used in the LDM simulation were used again with additional new waves generated for frequencies between the LDM and HDM Nyquist frequencies. The high- and low-resolution initial conditions were then combined with the former being used within the previously identified mask and the latter elsewhere. This resulted in 5 191 535 dark matter particles (as compared with 4 096 000 in the original low-resolution simulation).

Finally, a third set of initial conditions was generated that included both gas and dark matter in the high-resolution regions. To do this, a gas particle was added at the location of each high-resolution dark matter particle. The masses of the two were adjusted to give the same total mass as before and to give the universal dark matter to baryonic matter mass ratio. The dark matter and gas particles were given identical displacements and velocities. The total number of particles for this run was 6 443 575.

The hydrodynamics simulation used parameters identical to that for the *Radiative* model of MTKP02. In particular, it included radiative cooling with a time-varying metallicity $Z(t) = 0.3(t/t_0)$ $Z_{\odot}$, where t_0 is the current age of the universe (approximately 12.8 Gyr for this cosmology), using cooling tables from Sutherland & Dopita (1993). Neither pre-heating nor feedback were included in this run.

The simulations were run on 64 processors on the Cray T3E at the EPCC, using a parallel form of the AP^{3}M SPH code HYDRA (Couchman, Pearce & Thomas 1995)[1]. The box was $200 h^{-1}$ Mpc across and used cosmological parameters: $h_0 = 0.71$; $\sigma_8 = 0.9$; $\Omega_m = 0.35$; $\Omega_v = 0.65$ and $\Omega_b = 0.038$. The shape parameter for the fluctuation spectrum was fixed at $\Gamma = 0.21$ using the fitting function of Bond & Efstathiou (1984). The gravitational softening was set to $100/(1 + z) h^{-1}$ kpc until $z = 3$, after which it was held fixed at $25 h^{-1}$ kpc. The initial redshift was $z = 49$ and the highest-resolution run required 3706 time-steps to evolve to $z = 0$.

2.2 Cluster properties

The properties of the resimulated clusters at $z = 0$ are listed in Table 2. The virial radius is defined as the radius of a sphere, centred on the densest dark matter particle, that encloses a mean density of 317 (specifically $178 \Omega_m^{-0.55}$, Eke et al. 1998) times the background density (111 times the critical density). The virial mass, M_{vir}, is the mass enclosed by this sphere and the virial temperature is the mean specific energy (kinetic plus thermal) of the dark matter and gas, multiplied by $\mu m_H/k$, where $\mu m_H = 10^{-24}$ g is the mean molecular mass and k is the Boltzmann constant. The X-ray temperature is weighted by emission in the soft X-ray band (0.3–1.5 keV), excluding emission from within $50 h^{-1}$ kpc (i.e. physical, not comoving) of the cluster centre (hereafter referred to as cooling-flow corrected emission). The soft-band X-ray luminosity is converted into an estimated bolometric luminosity using the procedure described in MTKP02. The substructure statistic is defined as the separation between the centroid of the mass and the location of the densest dark matter particle, in units of the virial radius (Thomas et al. 1998). The formation expansion factor, a_f, is a characteristic formation epoch for the cluster as defined in Section 3.1.

---

[1] HYDRA is available from http://hydra.susx.ac.uk/

Table 2. Cluster properties: identifying number; virial radius in units of h^{-1} Mpc; virial mass in units of $10^{14} h^{-1}$ M$_\odot$; virial temperature in units of keV/k; substructure statistic; soft-band, emission-weighted temperature excluding emission within $50\,h^{-1}$ kpc of the cluster centre in units of keV/k; bolometric luminosity estimated from soft-band emission, excluding emission from within $50\,h^{-1}$ kpc of the cluster centre, in units $10^{44}h^{-2}$ erg s^{-1}; formation expansion factor as fit to the $M_{\rm vir}$ evolution – see Section 3.1. The clusters marked in bold are those that will be examined in detail below.

ID	$R_{\rm vir}$	$M_{\rm vir}$	$T_{\rm vir}$	T_X	L_X	Sub.	$a_{\rm f}$
1	2.41	17.85	9.62	7.15	9.22	0.11	0.671
2	**1.80**	**7.49**	**4.99**	**4.68**	**1.37**	**0.05**	**0.529**
3	1.79	7.33	4.63	3.41	1.13	0.14	0.718
4	1.78	7.26	5.09	5.09	1.73	0.02	0.688
5	1.67	6.02	3.75	3.07	0.43	0.12	0.890
6	1.62	5.46	4.04	4.09	1.04	0.07	0.557
7	1.62	5.44	3.61	3.10	0.38	0.19	0.756
8	**1.61**	**5.39**	**4.27**	**5.24**	**2.63**	**0.03**	**0.443**
9	1.61	5.34	4.70	3.94	1.93	0.15	0.845
10	1.60	5.25	4.09	4.33	1.36	0.02	0.459
11	**1.60**	**5.22**	**4.15**	**4.19**	**1.74**	**0.08**	**0.731**
12	1.59	5.13	4.37	4.58	2.19	0.03	0.565
13	**1.58**	**5.06**	**5.38**	**6.18**	**3.12**	**0.09**	**0.487**
14	1.56	4.83	3.83	3.77	0.52	0.25	0.774
15	1.54	4.71	3.41	4.11	1.27	0.06	0.535
16	1.54	4.71	3.15	3.00	1.14	0.11	0.777
17	1.53	4.61	4.59	4.19	1.92	0.06	0.501
18	1.53	4.58	3.62	4.27	0.84	0.03	0.699
19	1.51	4.43	3.48	4.38	0.99	0.05	0.480
20	1.35	3.17	3.13	3.60	1.02	0.06	0.401

Note that, after resimulation, the virial mass and temperature of the final cluster in the list dropped significantly. This is because the cluster is in the process of merging with a subcluster that lay just inside the virial radius in the original low-resolution run but has moved just outside it in the high-resolution run. Even so, this cluster still has over 13 000 particles each of gas and dark matter within the virial radius at the final time. The largest cluster has approximately 73 000 particles of each type at the end.

2.3 Testing

The mass of dark matter particles in the low-resolution regions exceeds that of those in the high-resolution regions by a factor of ∼9 (and of the gas particles by a factor of ∼74). It is therefore necessary to ensure that the clusters are not affected by these high-mass particles which could cause unphysical two-body relaxation (since the softening is the same for all the particles). The clusters were examined to discern if there were any low-resolution particles within their virial radii at any output time. It was found that only one of the clusters presented was at all affected. This was cluster 13, which temporarily has up to two low-resolution dark matter particles within the virial radius during a late-time merger. We do not expect this to affect the results and we choose to ignore it.

As a test of our method the clusters were compared with those from the *radiative* simulation of MTKP02. A comparison between the temperature–mass relation and the luminosity–temperature relation for the two is shown in Fig. 1. To be consistent with MTKP02, the extent of the clusters is defined by a sphere that encloses a mean density of 200 times the critical density. It is clear that the new clusters are consistent with the previous relations but extend them to higher mass and temperature.
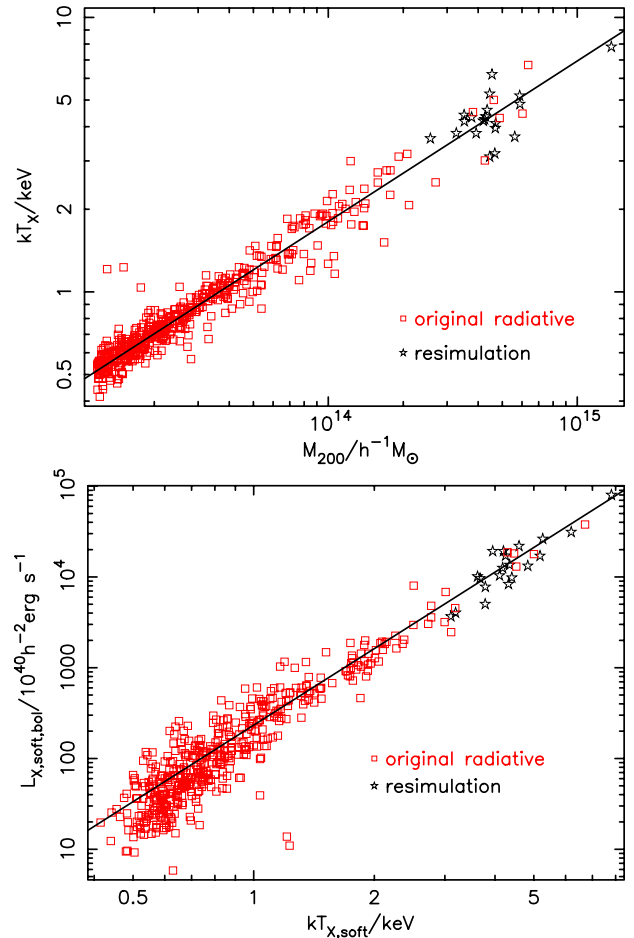

Figure 1. Cooling-flow corrected T_X–M_{200} (upper panel) and L_X–T_X (lower panel) relation in the soft X-ray band (luminosity has been converted into an estimation of the bolometric luminosity) for the clusters from MTKP02 (squares) and those from simulation HGAS (stars). The lines have a slope of 0.59 (upper panel) and 2.80 (lower panel).

One surprising result, however, is that the number of clusters above a virial temperature of 3 keV in the new runs is far fewer than eight times the number in the original MTKP02 simulation (20 as compared with seven) which was 1/8 of the volume. To test our normalization, we compare in Fig. 2 the mass-function of the simulated clusters with that predicted by Jenkins et al. (2001) from a compilation of a large number of N-body simulations. The 20 high-resolution clusters are contained in the final three bins of the plot (except for the most massive cluster that lies off the right-hand-side of the plot). In the same mass-range, three clusters are expected in the MTKP02 simulation but six are found. We put this down partly to chance and partly due to the fact that simulations do not sample waves correctly on scales comparable to the box-size.

3 THE TIME EVOLUTION OF MASS, X-RAY LUMINOSITY AND TEMPERATURE

In this section we look at the change in the mass, X-ray luminosity and X-ray temperature of the clusters as they evolve. For simplicity and for ease of physical interpretation, we use the bolometric (i.e. not the soft-band used above) emission from within the virial radius in the rest-frame of the cluster.
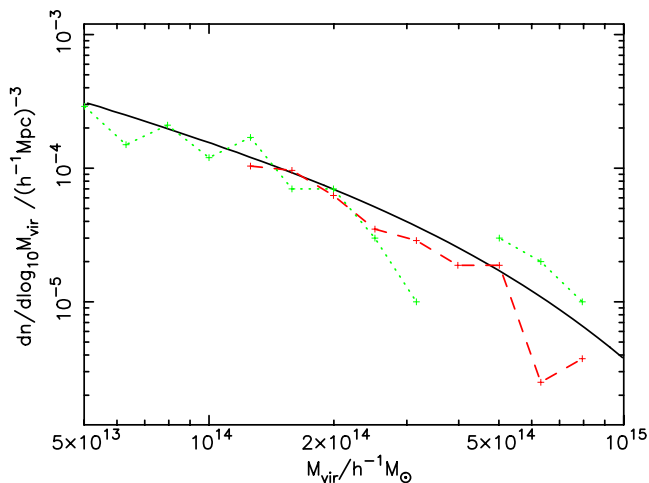
Figure 2. The mass function of clusters in the LDM simulation (dashed line) and in the simulations of MTKP02 (dotted line) compared with the prediction from Jenkins et al. (2001) (solid line). The most-massive cluster lies off the right-hand-side of the plot and has not been included in the figure as there are numerous empty bins between it and the second most-massive cluster.

The time resolution is defined by the light crossing time of half the box, that is $0.5 \times 200\,h^{-1}$ Mpc $\times\, a/c \approx 4.6 \times 10^8 \times a$ yr, where c is the speed of light and $a = 1/(1 + z)$ is the expansion factor. These times were chosen to match previous simulations that were used to obtain light-cones. This gives sufficient resolution to crudely resolve the mergers for the clusters as a whole, although finer time-resolution would have allowed us to examine accretion into the cores of the clusters in more detail.

3.1 The growth of mass

Fig. 3 shows the time-development of the mass enclosed within $R_{\rm vir}$. The most-massive cluster is located in the top-left panel of this figure (and also in Figs 4–6), with successively smaller clusters reading from left-to-right and then top-to-bottom as numbered. The plots go back to a time ($a = 0.35$) when the smallest cluster has a virial mass of $1.5 \times 10^{13} h^{-1}$ M$_\odot$, corresponding to 600 particles of each species. Also shown is M_{500}, the mass enclosed by a sphere within which the mean density is 500 times $\rho_{c0}(1 + z)^3$, where ρ_{c0} is the critical density at $z = 0$.

It is apparent from this figure that there are times when the mass of a cluster increases smoothly and other times when it undergoes sudden jumps; we designate these as minor and major mergers, respectively. Although the division between the two is somewhat arbitrary, it is a useful one, as we will show below that X-ray cluster luminosity evolves quite differently in the two regimes. For the purposes of this paper we define the onset of a major merger as occurring when the jump in $\log_{10} M_{\rm vir}$ between one output time and the next is 0.08 or more (i.e. a factor of 1.2). Visual inspection of the luminosity and temperature evolution suggests that the effects of a major merger last for three successive output times, approximately $1.4 \times 10^9 \times a$ yr. This roughly corresponds to the dynamical time of the clusters, although it does not scale in quite the same manner ($\propto a$ instead of $\propto a^{3/2}$). The jump criterion of 0.08 is chosen such that, averaged over all the clusters, approximately half of the mass is accreted during major and half during minor mergers. On average, approximately 25–30 per cent of the cluster outputs correspond to periods of major merger activity.

From Fig. 3, it can be seen that clusters exhibit a wide variety of formation histories. Some (e.g. clusters 9 or 16) acquire most of their mass in major mergers, while others (clusters 2 and 20) undergo no major mergers at all. The percentage increase of logarithmic mass during major mergers is show in the figure and summarized as a histogram in Table 3.

It is common in the literature (Lacey & Cole 1994; Navarro, Frenk & White 1997) to tacitly assume that cluster properties are fixed at the time of formation and remain unchanged since then. However, only in a minority of cases is it possible to assign a particular 'formation time', associated with a major merger, to the cluster. An alternative approach has been suggested by Wechsler et al. (2002) who fitted models of the form $M(a) = M_0\, e^{2a_f(1-1/a)}$ to the data. The point where the slope of the relation equals 2 defines a characteristic formation epoch for each cluster, as listed in Table 2. We shall investigate later, in Section 4, whether the X-ray properties of clusters are correlated with their formation time.

The growth in $M_{\rm vir}$ is relatively monotonic although there is sometimes a slight decline after a merger. The rises in M_{500} occur later and are often followed by a decline as the central regions of a cluster settle down after the merger. For this reason, it may be thought that $M_{\rm vir}$ is a more useful measure of the mass of a cluster. However, it will be shown in Section 4 that the X-ray properties are more closely correlated with M_{500}, because the bulk of the X-ray emission originates in this central region.

3.2 Long-term trends in X-ray properties

Figs 4 and 5 show the time-development of the bolometric luminosity and emission-weighted temperature of the clusters. The thick line shows the total emission and the thin line shows cooling-flow corrected emission.

These figures show that the X-ray temperature and the luminosity of each cluster are undergoing continual fluctuations associated with both major and minor mergers. These tend to obscure the long-term trends, and so we have defined smoothed versions of these plots in which the average profiles are defined as the median from each set of five successive output times.

Fig. 6 shows the trajectory of the smoothed X-ray properties for each cluster in the luminosity–temperature plane. Also displayed are the fractional logarithmic mass accreted during major mergers, and vectors indicating the overall drift of the cluster across the L_X–T_X plane. It can be seen that the clusters that accrete only a small amount of mass during major mergers tend to move down and to the right (i.e. they become less luminous with time), whereas those that accrete most of their mass in this way move up and to the right (i.e. they become more luminous). This is confirmed by the statistics in Table 3 that show the average direction of motion across the L_X–T_X plane in four bins corresponding to different fractional logarithmic mass accreted during major mergers.

For the majority of their lives, between major mergers, clusters grow dimmer and heat up (on average increasing their temperature by 0.20 in the log with a gradient in the $\log L_X - \log T_X$ plane of -1.46) so that the normalization of the L_X–T_X relation decreases with time. During major mergers, clusters become brighter and hotter (on average increasing their temperature by 0.26 in the log with a gradient of 1.54). If we allow for the time the mergers take then this motion is roughly parallel to the mean relation ($L_X \propto T_X^{2.8}$). This would suggest the merger history of clusters does not induce significant scatter in the relation. Thus we can think of the mean L_X–T_X relation as gradually drifting to lower normalization as time
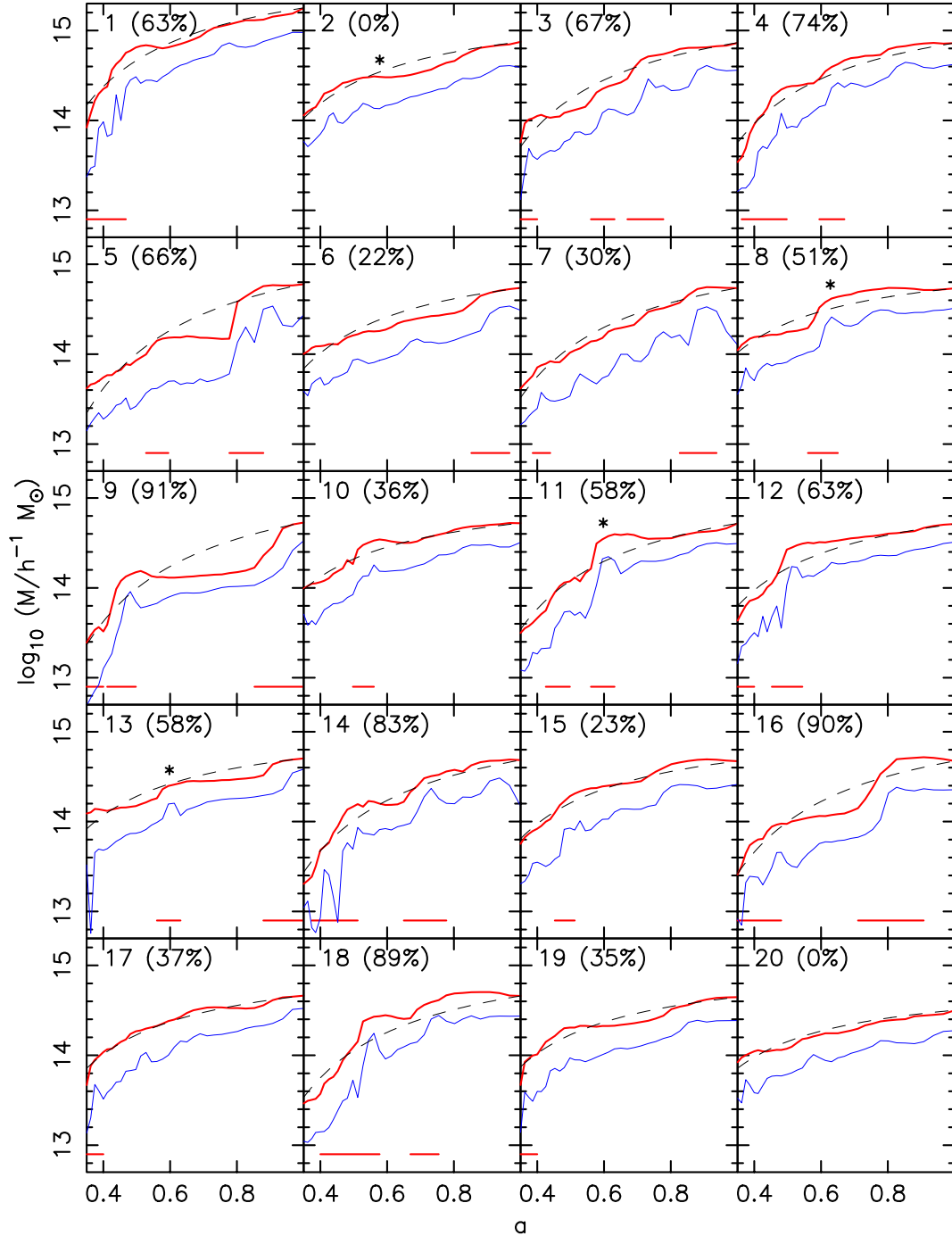
Figure 3. M_{vir} (thick line) and M_{500} (thin line) versus the expansion factor for the clusters. The dashed curves are a one-parameter fit to the functional form $M(a) = M_0 \, e^{2a_{\mathrm{f}}(1-1/a)}$ introduced by Wechsler et al. (2002), where a_{f} is listed in Table 2. The asterisks indicate events that will be investigated in detail below. The lines along the bottom of each box indicate the times during which the cluster is deemed to be undergoing a major merger (as defined in the text). The numbers in parentheses indicate the fractional logarithmic mass accreted during major mergers.

increases. Major mergers do not affect this drift but shift individual clusters along the relation to higher temperature and luminosity.

Simple scaling arguments suggest that $L \propto M\rho T^{1/2}$ where M is the cluster mass, ρ the density and T the temperature. (Note that the dominant contribution to the flux comes from the region where $\rho \propto r^{-3/2}$, so this defines the characteristic size to use in the scaling relation.) For the population as a whole one would expect the luminosity to decrease with time, at fixed mass, as the characteristic

density decreases roughly in proportion to the mean density of the Universe. However, for individual clusters, the increase in mass more than makes up for this. However, as we have seen above, the increase in luminosity is not smooth. During major mergers the mass increases abruptly. There will be an influx of cool, low-entropy gas and much of this will reach the core, causing a long-term increase in luminosity. Between major mergers the mass continues to increase but the influx of low-entropy gas is insufficient to replenish gas lost
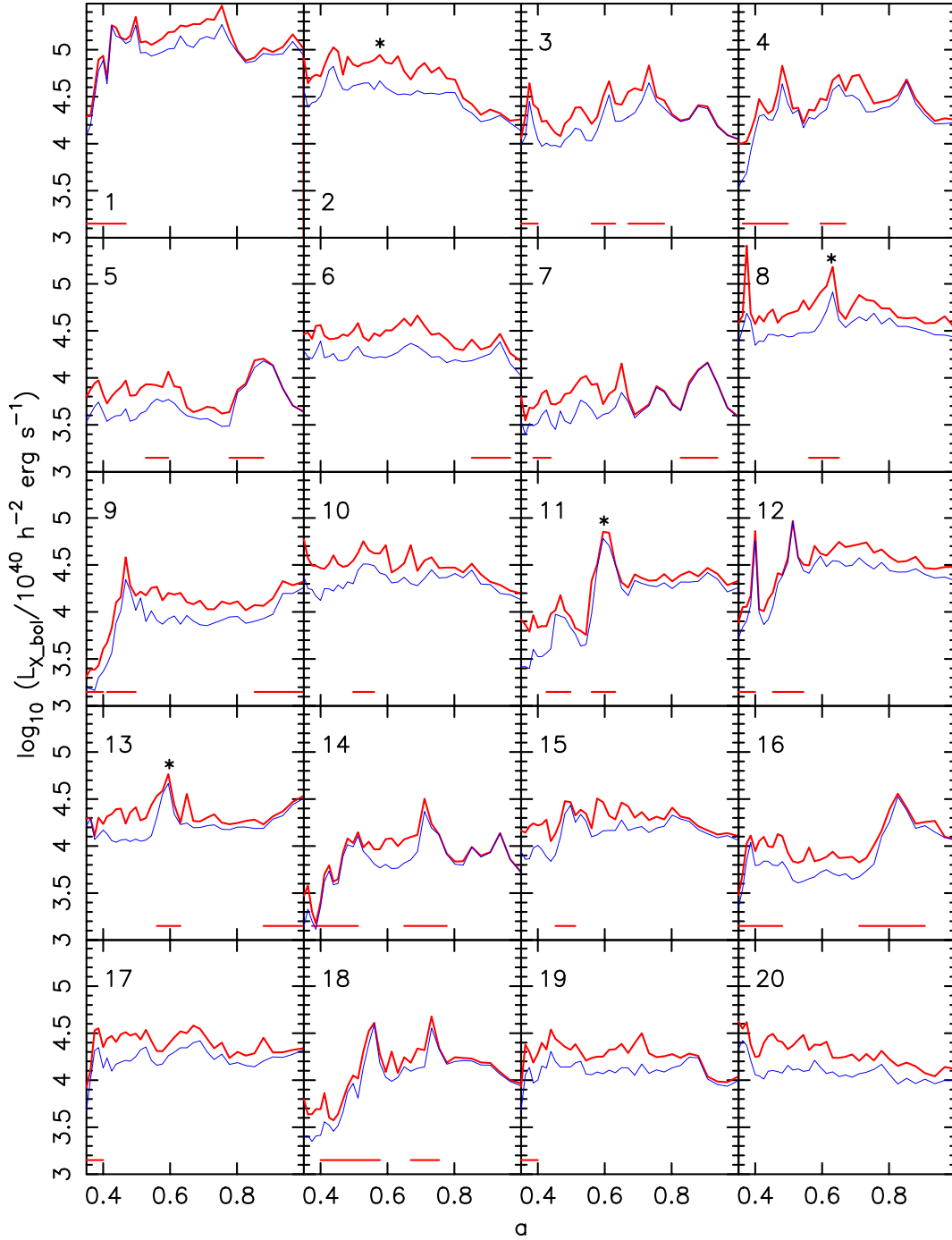
Figure 4. Bolometric luminosity versus the expansion factor for the clusters. The thick line shows the total emission; the thin line shows cooling-flow corrected emission. The asterisks indicate events that will be investigated in detail below. The lines along the bottom of each box indicate the times during which the cluster is deemed to be undergoing a major merger.

by radiative cooling and the core density and luminosity decrease. This will be looked at in more detail in a future paper.

3.3 Short-term fluctuations in the X-ray properties

We next turn from the long-term behaviour of the smoothed temperature and luminosity profiles to look at the fluctuations during mergers. These exhibit a variety of behaviours that we shall illustrate with specific examples drawn from our simulations. Figs 7,

9, 11 and 13 show maps of several example clusters at different expansion factors as indicated in the captions. The maps are generated in the same manner as in Onuora, Kay & Thomas (2003). The half-width of each map is equal to the virial radius and the emission is projected along the line of sight on each side of the clusters to a depth equal to twice the virial radius. The contours show X-ray surface brightness and are separated by 0.2 dex; the colours indicate emission-weighted temperature; and the arrows show the mass-weighted bulk flow, normalized to the highest velocity grid
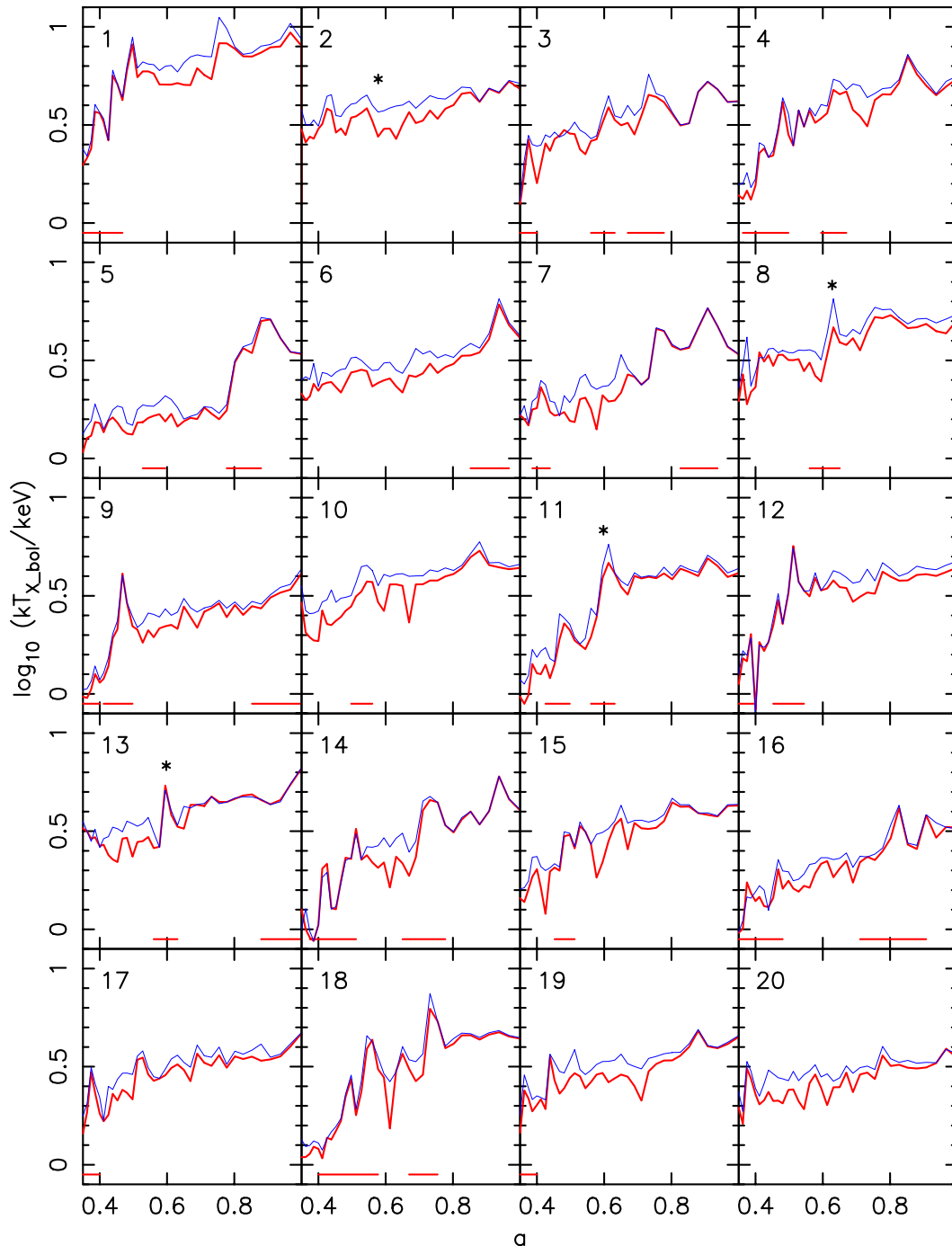
Figure 5. Bolometric emission-weighted temperature versus the expansion factor for the clusters. The thick line shows temperature calculated using the total emission; the thin line using cooling-flow corrected emission. The asterisks indicate events that will be investigated in detail below. The lines along the bottom of each box indicate the times during which the cluster is deemed to be undergoing a major merger.

point. The corresponding evolution in the luminosity–temperature plane is shown in Figs 8, 10, 12 and 14; in order to show the relative size of fluctuations, these figures all have the same dynamic range.

3.3.1 Slow accretion

Even when not undergoing major mergers, clusters still show fluctuations in their luminosity and temperature evolution. However, these are reduced if emission from within $50\,h^{-1}$ kpc of the cluster

core is excluded (see Table 4). What is happening is that the clusters are growing by accretion of small subclumps and the fluctuations are due to emission from low-entropy gas that makes its way to the cluster core and cools rapidly. This sometimes causes a temporary decrease in the temperature of the cluster core, such as the two dips in the temperature of cluster 10 at expansion factors of 0.60 and 0.67.

Cluster 2, the second most-massive cluster in our sample, has accreted all its mass during minor mergers. Fig. 7 shows snapshots at
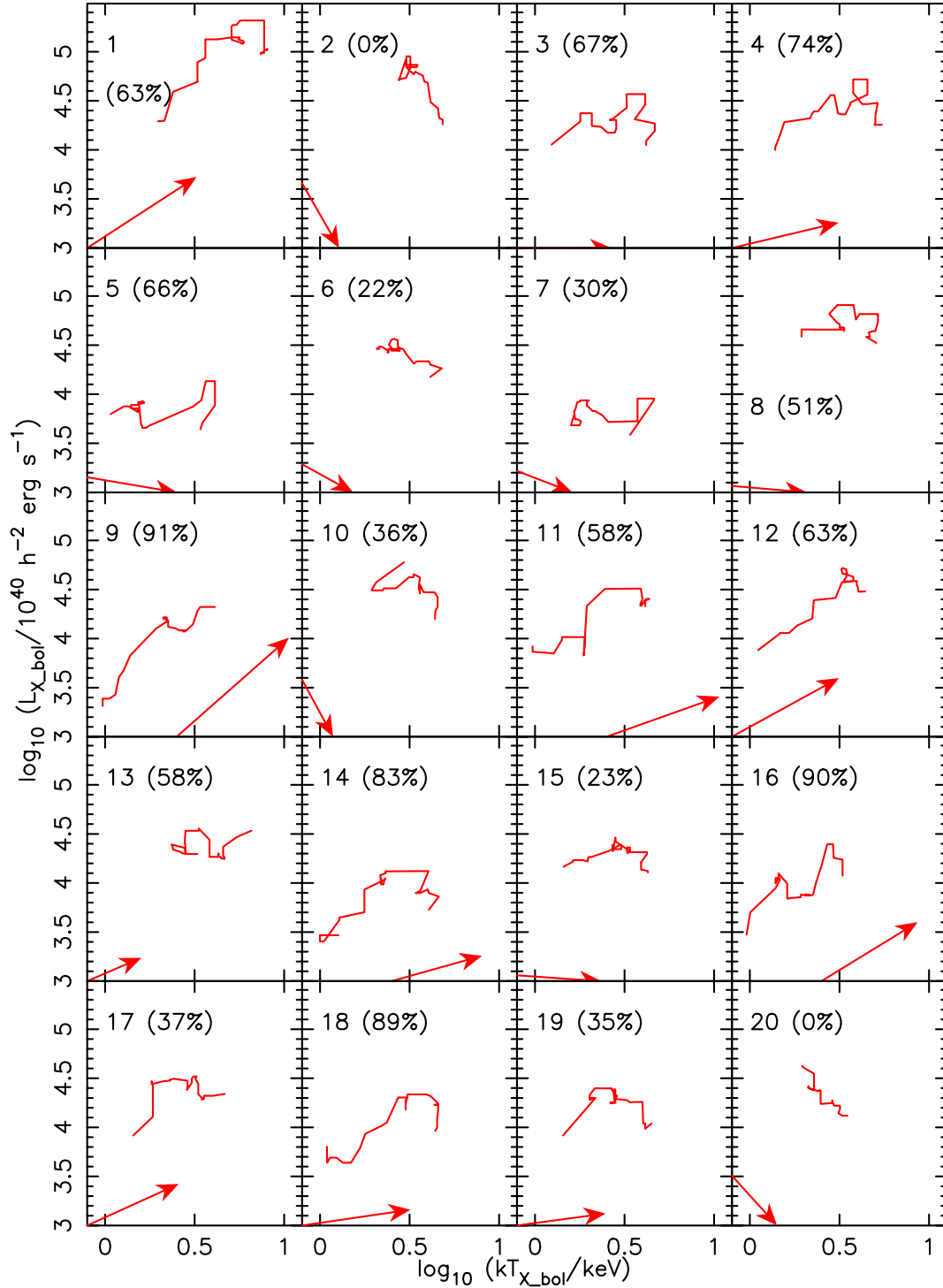
Figure 6. The time-development of the smoothed bolometric luminosity versus emission-weighted temperature for the clusters. The arrows show the overall drift of the cluster in the L_X–T_X plane. The bracketed numbers indicate the fractional logarithmic mass accreted during major mergers.

$a \approx 0.56$ in which the infall of small subclumps is clearly visible. The substructure statistic is less than 0.1 throughout the evolution of the cluster, indicating that the subclumps are too small to significantly displace the centre of mass. Even so, the accretion gives rise to small-scale scatter as seen in Figs 4, 5 and 8. At any particular time, most clusters show this kind of low-level activity similar to the minor mergers investigated by Motl et al. (2003).

3.3.2 Single-peaked major mergers

The most-common behaviour seen in major mergers is a temporary upward fluctuation in luminosity that is usually accompanied by an increase in temperature (the residuals of L_X and T_X have a Spearman rank coefficient of 0.48, which corresponds to a correlation with a significance of over 99.9 per cent). Many examples of this can be

Table 3. Number of clusters accreting various fractions of their material through major mergers. Also shown is the mean angle (with respect to positive T_X evolution and no L_X evolution) in log space, which the clusters move across the L_X–T_X plane (see Fig. 6).

Fraction accreted during mergers	$\geqslant 0$ per cent <25 per cent	$\geqslant 25$ per cent <50 per cent	$\geqslant 50$ per cent <75 per cent	$\geqslant 75$ per cent $\leqslant 100$ per cent
Number of clusters	4	4	8	4
Mean angle of L_X–T_X drift	$-47°$	$14°$	$21°$	$38°$
Mean d log L_X/d log T_X	-1.07	0.25	0.38	0.78
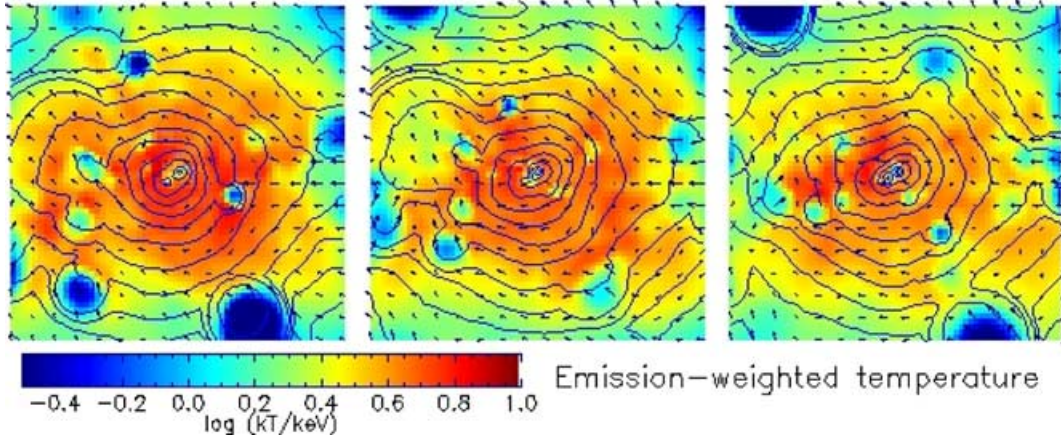
Figure 7. Surface-brightness and emission-weighted temperature map for cluster 2, as described in the text. The panels are at $a = 0.544$, 0.560 and 0.577 so there is approximately 2.6×10^8 yr between panels. The virial radius increases from $0.84\, h^{-1}$ Mpc in the first panel to $0.88\, h^{-1}$ Mpc in the third panel.
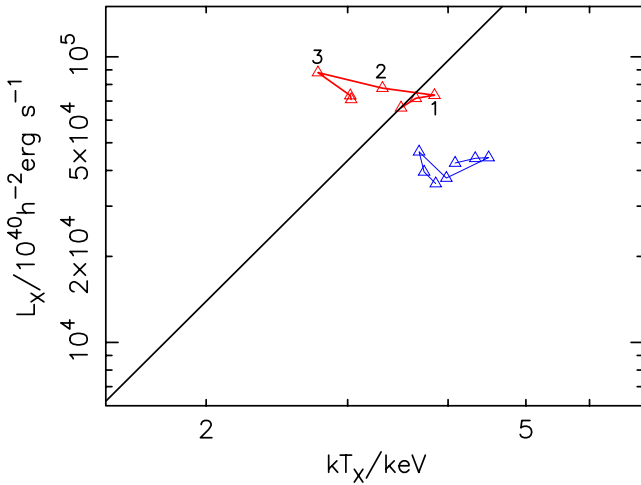

Figure 8. Evolution in the L_X–T_X plane of cluster 2 over the time shown in Fig. 7. The panels in Fig. 7 correspond to the numbers 1–3 here. The thick line plots properties for the whole cluster and the thin line plots cooling-flow corrected L_X and T_X. The straight solid line shows a power-law relation of the form $L_X \propto T_X^{2.8}$.

detected in Figs 4 and 5. These fluctuations are not restricted to the core and correspond to more violent mergers that boost the luminosity of the whole cluster through compression of the intracluster medium.

Figs 9 and 10 show an example from cluster 8 at $a \approx 0.63$. This is caused by an approximately equal-mass merger (of clusters with masses 1.82×10^{14} and $1.41 \times 10^{14}\, h^{-1}$ M$_\odot$) that produces a planar compression front perpendicular to the direction of the merger. The planar nature of the front can be more or less obvious than that shown here, depending upon the impact parameter of the collision, the degree of substructure and the viewing angle.

3.3.3 Double-peaked major mergers

Sometimes a merger will be associated with a double peak in the luminosity, the first associated with an increase in temperature and the second a decrease. This happens when the cores of the main cluster and the in-falling subcluster do not merge directly but orbit about each other for a while before doing so. Unfortunately, the time resolution of our outputs is insufficient to determine whether this is the generic behaviour.

Fig. 11 shows a major merger of this type in cluster 13 at $a \approx 0.6$. In the first two panels the subclump approaches and in the third panel the clusters collide and the temperature and luminosity peaks. At the time of maximum luminosity, however, the surface brightness contours are relatively round and there is little evidence from the surface-brightness alone that a merger is taking place (the asymmetry that is visible in the figure is from in-falling matter that does not contribute significantly to the luminosity and temperature variation). The cores have not lost all relative momentum, however, and so they reseparate and do not fully merge until the final panel. This brings about a second peak in the luminosity, which is only observed in the core (see Fig. 12). Since this is relatively cool, the X-ray temperature drops at this point before stabilizing at a higher value. Note that, at the point at which the cores merge, the cluster again looks fairly spherical and relaxed.

This is the behaviour observed in the toy models of Ritchie & Thomas (2002). The largest peak in the luminosity in these
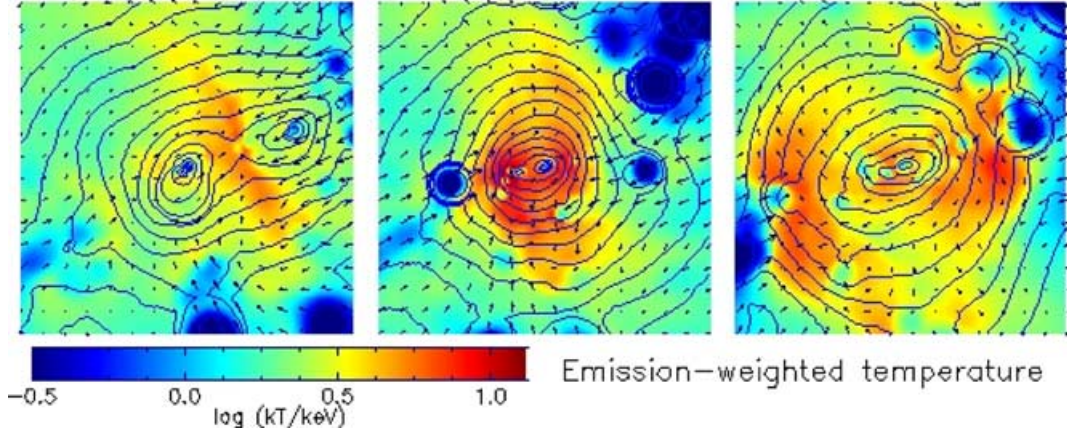
Figure 9. Surface-brightness and emission-weighted temperature map for cluster 8, as described in the text. The panels are at $a = 0.595$, 0.631 and 0.670 so there is approximately 5.8×10^8 yr between panels. The virial radius increases from 0.68 h^{-1} Mpc in the first panel to 0.76 h^{-1} Mpc in the third panel.
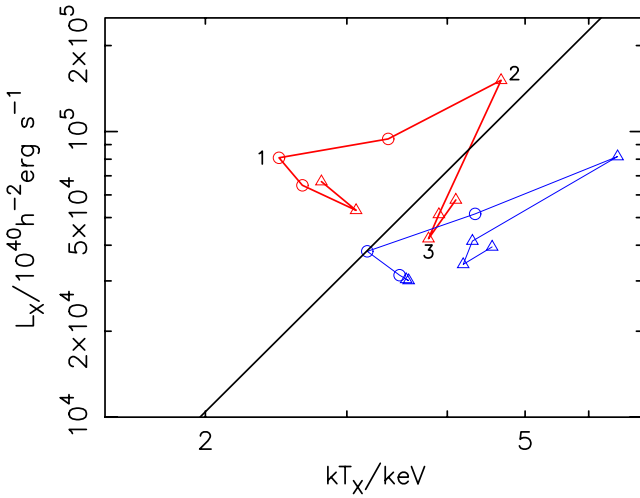

Figure 10. Evolution in the $L_X–T_X$ plane of cluster 8 when it undergoes the merger shown in Fig. 9. The panels in Fig. 9 correspond to the numbers 1–3 here. The circles correspond to times when the cluster has a substructure statistic greater than 0.1; other times are marked with triangles. The thick line plots properties for the whole cluster and the thin line plots cooling-flow corrected L_X and T_X. The straight solid line shows a power-law relation of the form $L_X \propto T_X^{2.8}$.

simulations was when the clusters first collided. Then the luminosity dropped as the core expanded again and then increased to a stable level as the core finally settled. This behaviour was more pronounced in off-axis collisions where the cores missed each other on the first pass.

3.3.4 Major mergers leading to a permanent increase in luminosity

Finally, there are major mergers that cause a permanent jump in luminosity and temperature after the initial fluctuation associated with the merger has died away. Half of the mergers involve a jump in the smoothed L_X (i.e. a permanent jump in L_X) of over a factor of 2 and half of the mergers involve a jump in the smoothed T_X of more than a factor of 1.4.

Fig. 13 shows images before, during and after one such merger, which cluster 11 undergoes at $a \approx 0.6$. There is a small amount of

hot, compressed gas as the subclump approaches, but not so obviously planar as in some other mergers. At the point of merging the cluster looks fairly relaxed in this projection although the substructure statistic is greater than 0.1 throughout.

Fig. 14 shows that L_X and T_X increase together approximately parallel to the $L_X–T_X$ relation in an elongated, clockwise ellipse. This is because the luminosity increases when the clump crosses R_{vir}, before it has had a chance to interact strongly with the ICM and raise the temperature of the gas. A similar effect is seen in Fig. 10 and the first (main) merger in Fig. 12

4 SCATTER IN THE X-RAY SCALING RELATIONS

To a greater or lesser degree all of the X-ray scaling relations show scatter both in observations and simulations. Some of this will be due to observational errors and resolution effects. However, as clusters have differing merger histories and are not self-similar, it is apparent that some, perhaps most, of this scatter is physical. As Figs 4 and 5 show, much of the scatter in luminosity and temperature comes from gas within 50 h^{-1} kpc of the cluster centre. For this reason, we omit the central gas when plotting the scaling relations.

Fig. 15 shows the current X-ray temperature–mass relation within R_{vir} (top panel) and R_{500} (bottom panel). The straight line is the best-fitting relation to a straight line of slope 0.60 in log space. This slope was chosen to agree with that from the clusters in MTKP02 which cover a much wider dynamic range in mass. We have investigated a wide variety of properties to try to find the main cause of the scatter; these include the following.

(i) The most obvious source of scatter is the fluctuations in temperature associated with mergers, i.e. the difference between the actual temperature and the smoothed temperature. However, this is currently of a magnitude (approximately 0.03 dex) that is too small to have much of an effect. We have looked for a correlation in these fluctuations and deviations from the temperature–mass relation, and find none.

(ii) The fractional logarithmic mass accreted during major mergers is also uncorrelated to scatter.

(iii) Wechsler et al. (2002) found a correlation between cluster formation time and the concentration of the dark matter. We used their method to assign characteristic formation epochs to each cluster (see Table 2) but again found no correlation with scatter.
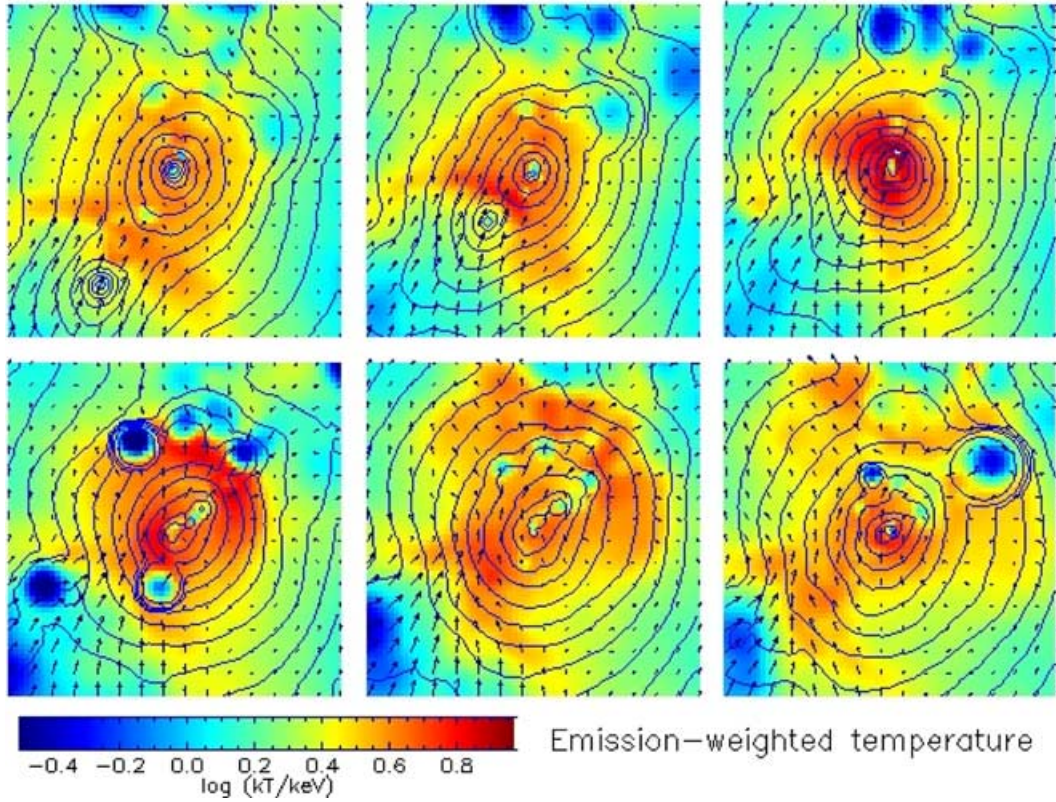
Figure 11. Surface-brightness and emission-weighted temperature map for cluster 13, as described in the text. The first panel is at $a = 0.560$ and the last is at $a = 0.650$ so there is approximately 2.8×10^8 yr between each panel. The virial radius increases from $0.72\ h^{-1}$ Mpc in the first panel to $0.95\ h^{-1}$ Mpc in the sixth panel.
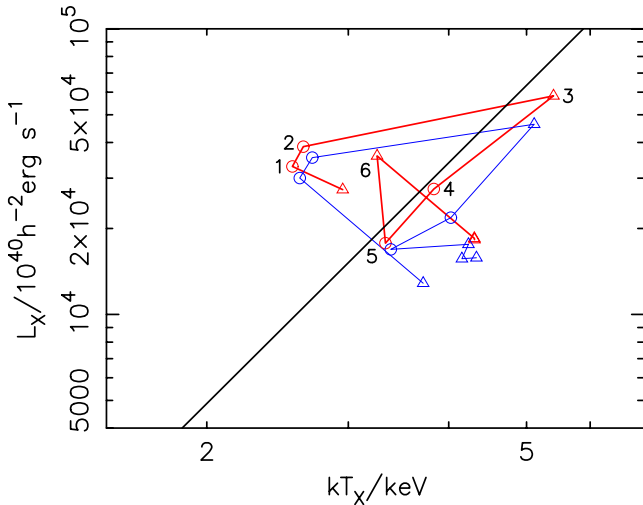

Figure 12. Evolution in the L_X–T_X plane of cluster 13 when it undergoes the merger shown in Fig. 11. The panels in Fig. 13 correspond to the numbers 1–6 here. The circles correspond to times when the cluster has a substructure statistic greater than 0.1; other times are marked with triangles. The thick line plots properties for the whole cluster and the thin line plots cooling-flow corrected L_X and T_X. The straight solid line shows a power-law relation of the form $L_X \propto T_X^{2.8}$.

(iv) The rate of increase of mass of both the cluster as a whole and of the core mass, averaged over different time periods before the present. This was also unsuccessful.

In the end, only one of the statistics that we looked at gave a strong correlation with scatter from the X-ray temperature–mass relation and that was the degree of substructure. The substructure statistic, defined as the separation between the position of the centroid and the dark matter density maximum in units of the cluster radius, is listed in Table 2. (Note that this statistic is a function of the cluster radius; the values in the table are for properties averaged within the virial radius.) The substructure statistic has several advantages over some of the other measures that we tried: it is relatively simple to calculate, it depends only upon the properties of the cluster at the present day, and it is closely related to some observable quantity (for example Schuecker et al. 2001 observed substructure in 52 ± 7 per cent of clusters from the REFLEX+BCG sample).

In Fig. 15, clusters with a substructure statistic greater than 0.1 are plotted as circles. It is immediately apparent from the upper panel that a large part of the scatter is related to substructure (formally, the distance below the line correlates to a substructure with a Spearman rank coefficient of 0.485, a significance of more than 95 per cent). It is interesting that most clusters with substructure scatter low on this plot. Some of these contain subclumps that are falling into the cluster for the first time and that have raised its mass without yet significantly altering the emission-weighted temperature; others are clusters which are undergoing a core-bounce after a merger and for which the temperature is temporarily slightly too low.

It is apparent from the larger scatter in the upper panel of Fig. 15, that the virial mass cannot be accurately determined from the X-ray properties a cluster when spatial information is not available. However, we can reduce the scatter considerably by moving to a more compact radius (see Table 5). This has several
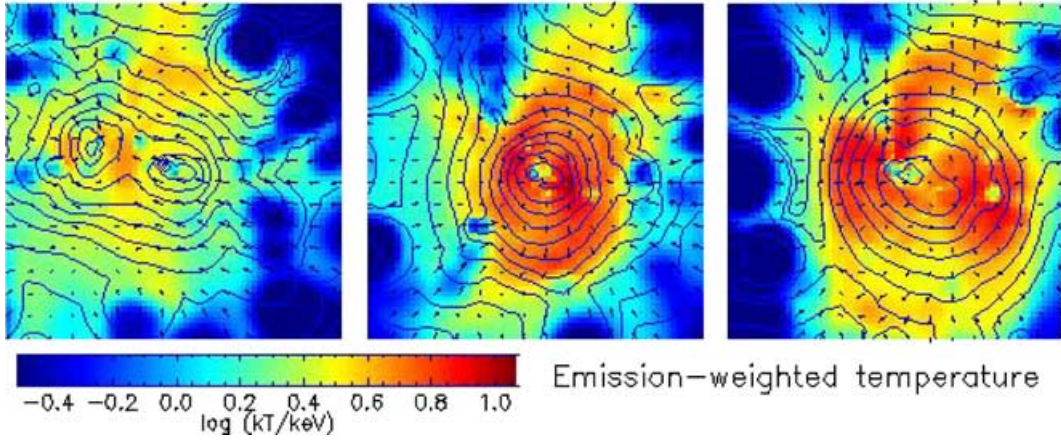
Figure 13. Surface-brightness and emission-weighted temperature map for cluster 11, as described in the text. The panels are at $a = 0.577, 0.613$ and 0.631 so there is approximately 5.5×10^8 yr between the first two panels and approximately 2.9×10^8 yr between the second and third panels. The virial radius increases from $0.89 \ h^{-1}$ Mpc in the first panel to $1.04 \ h^{-1}$ Mpc in the third panel.
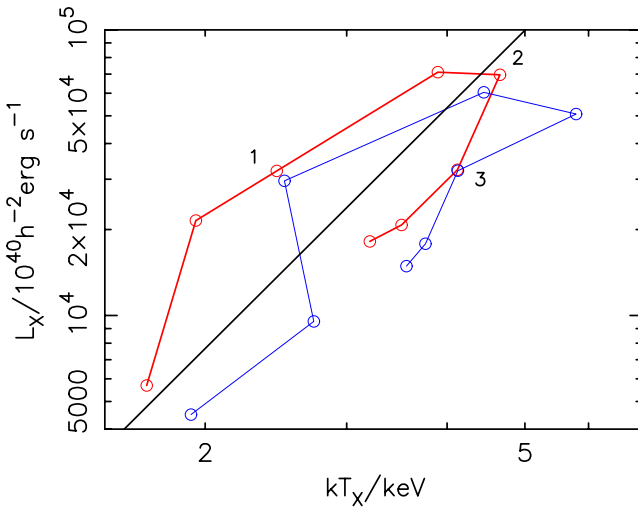

Figure 14. Evolution in the L_X–T_X plane of cluster 11 when it undergoes the merger shown in Fig. 13. The panels in Fig. 13 correspond to the numbers 1–3 here. The thick line plots properties for the whole cluster and the thin line plots cooling-flow corrected L_X and T_X. The straight solid line shows a power-law relation of the form $L_X \propto T_X^{2.8}$.

advantages: the number of clusters showing substructure is reduced, the properties are measured at radii that are more accessible to X-ray observations, and the substructure that is measured is more directly related to subclumps that are interacting strongly with the intra-cluster medium and that will be influencing the X-ray properties.

The lower panel in Fig. 15 shows the T_X–M_{500} relation. As can be seen, the relation is much tighter than before, and interestingly, the scatter of high substructure clusters from the relation is much-reduced. The circle that lies furthest above the solid line is cluster

Table 4. Rms change in the log of the bolometric luminosity and temperature between one output time and the next, excluding times during major mergers.

Property	Total	Cooling-flow corrected
Luminosity	0.120	0.090
Temperature	0.069	0.059

13, which has recently merged and where the temperature is still enhanced by the associated compression of the ICM. This cluster was even further from the line in the original plot (the topmost large triangle), but did not show up as having substructure because the subclump was too close to the centre. The circle that lies furthest below the line in the bottom panel is cluster 5 which temporarily has a cooler temperature than the average due to core expansion following a recent merger.

Note that, for most of the clusters, the mass decreases slightly in the move from R_{vir} to R_{500}, but for the two leftmost clusters in the bottom panel (clusters 7 and 14) it changes significantly. It can be seen from Table 2 that these are the two clusters with the highest degree of substructure at the end. What has happened is that while R_{vir} encloses the subclump causing the substructure R_{500} does not. The luminosity of these clusters also decreases significantly and they would be easily seen as bimodel in any X-ray observation. For this reason, we omit them from the scatter statistics listed in Table 5.

Having eliminated the principal cause of the scatter in the T_X–M relation, we again tested to see whether any of the properties considered earlier now correlate with the residual scatter, but with negative results.

Figs 16 and 17 show equivalent plots for the luminosity–mass and luminosity–temperature relations. The former has a similar variation to substructure as seen in the temperature–mass relation. The latter shows no obvious correlation of scatter with substructure, consistent with our earlier observation that motion in the L_X–T_X plane during mergers tends to be parallel to the mean relation. However, in the upper panel of Fig. 17 there is a concentration of clusters toward the bottom-left showing substructure. This reflects the fact that the sample was selected on the basis of virial mass and contains a number of clusters for which the merging is not complete. Conversely, in any X-ray luminosity or temperature-limited sample there will be a bias against high virial mass clusters with a high degree of substructure. This bias is reduced when properties are measured within R_{500} instead.

5 DISCUSSION

In this study, the formation of 20 large clusters of galaxies has been followed by resimulating the regions around them at high resolution. The X-ray properties were found to vary with time, driven
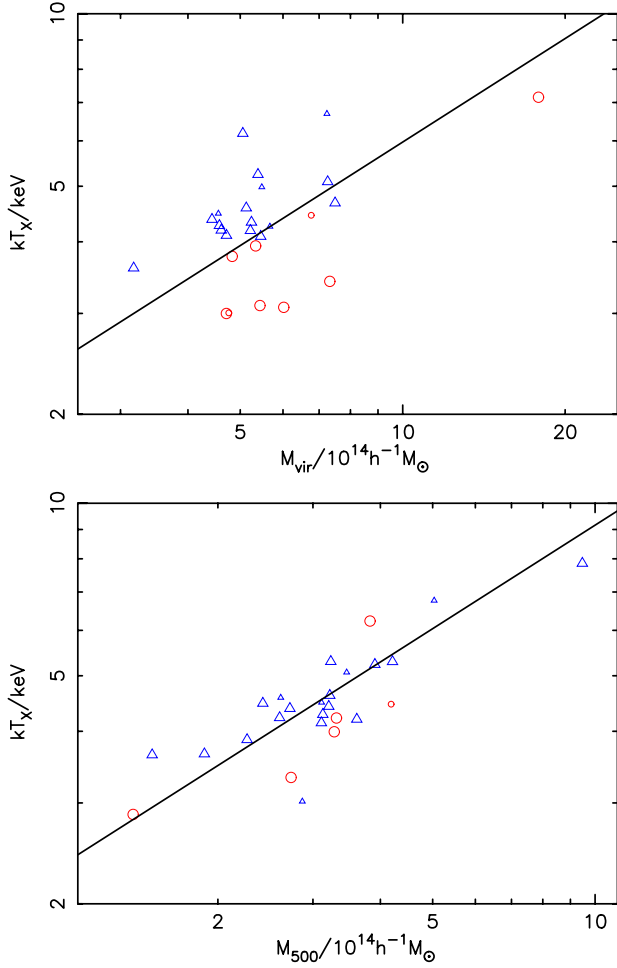
Figure 15. Cooling-flow corrected soft-band X-ray temperature versus mass. In the upper panel the outer radius of the cluster is $R_{\rm vir}$; in the lower panel it is R_{500}. The solid lines are fits to the data of a power-law relation $T_X \propto M^{0.60}$. The circles represent clusters for which the substructure statistic is greater than 0.1; other clusters are indicated with triangles. Large symbols represent the resimulated clusters presented in this paper; small symbols are clusters from MTKP02.

mainly by the merging history of the clusters. Accretion during major mergers tends to increase the luminosity of a cluster, pushing it up the L_X–T_X relation, while between major mergers it slowly decreases, following the movement of the L_X–T_X relation. In addition to this long-term variation, there are short-lived fluctuations associated with the merger itself.

Over the period investigated clusters were said to be undergoing a major merger approximately 25–30 per cent of the time. However, to convert this to a number that can be compared with X-ray observations is very complex. First, our definition of a major merger

Table 5. Scatter about the fits to the plots in Figs 15–17. This is defined as the rms deviation in the vertical direction in dex after allowing for the one free parameter in the fit.

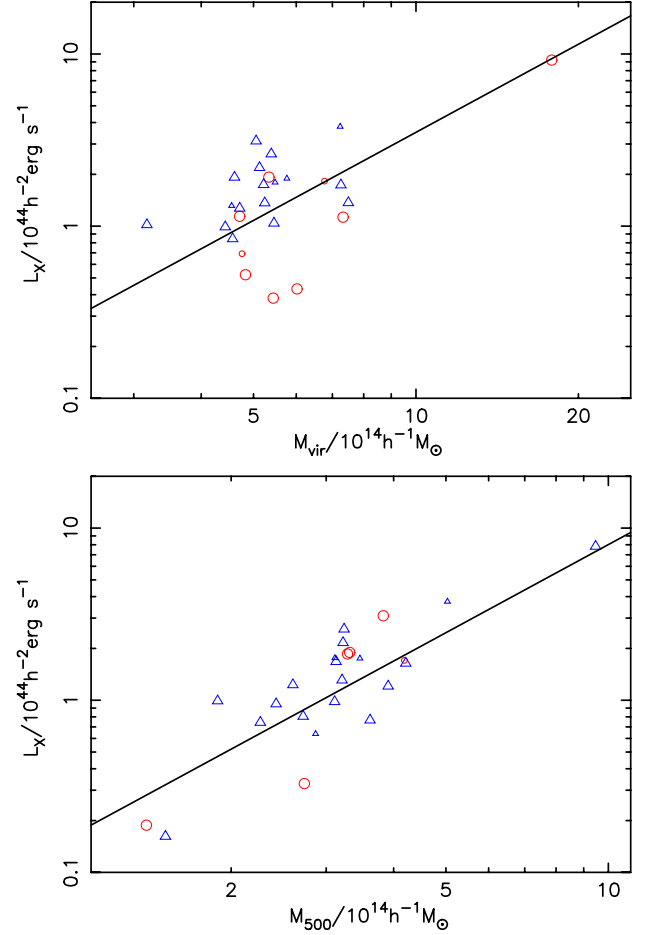| Relation	Scatter in $R_{\rm vir}$ values	Scatter in R_{500} values
T_X–M	0.088	0.057
L_X–M	0.25	0.19
L_X–T_X	0.16	0.15

Figure 16. Cooling-flow corrected bolometric X-ray luminosity estimated from emission in the soft band versus mass. In the upper panel the outer radius of the cluster is $R_{\rm vir}$; in the lower panel it is R_{500}. The solid lines show power-law relations of the form $L_X \propto M^{1.7}$. The symbols have the same meaning as in Fig. 15.

was very ad hoc and a more detailed comparison of possible definitions with X-ray observability would be required. In addition, there will be strong selection effects that favour high-redshift clusters undergoing temporary boosts in X-ray luminosity. A detailed investigation of these biases will be required in order to correctly interpret observations of the X-ray properties of clusters at high redshift.

As a subclump crosses $R_{\rm vir}$, the mass and the luminosity increase, but the temperature stays roughly constant or decreases slightly (since the subclump will be cooler than the cluster). This causes the cluster to move below the T_X–M and L_X–M relations and so clusters with structure within $R_{\rm vir}$ tend to be scattered low on the plots. For this reason, the mass within a smaller region such as R_{500} correlates more closely with X-ray properties than does the virial mass.

As the subclump moves through the ICM of the cluster, it compresses the gas in front of it. This causes adiabatic heating and can be observed as a hot planar compression front. These features have been observed, for example by Maughan et al. (2003). Fig. 5 from their paper shows surface-brightness contours from a *Chandra* map of Cl J0152.7-1357 a cluster at $z = 0.833$ and shows that the cluster is undergoing a major merger. Fig. 11 from the same paper shows the hardness of the X-rays with lighter regions representing harder
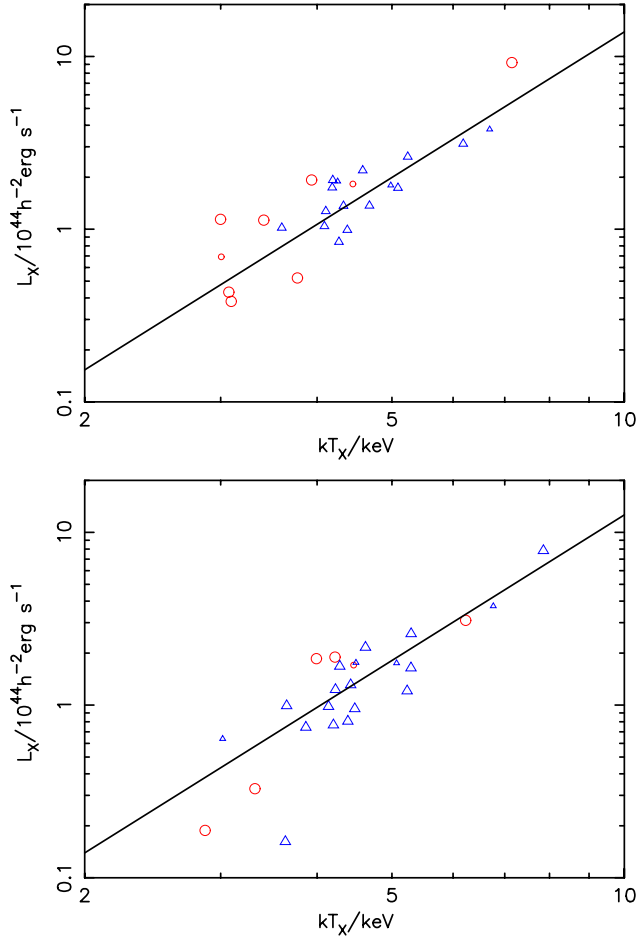
Figure 17. Cooling-flow corrected bolometric luminosity versus X-ray temperature estimated from emission in the soft band. In the upper panel the outer radius of the cluster is $R_{\rm vir}$; in the lower panel it is R_{500}. The solid lines show power-law relations of the form $L_X \propto T_X^{2.8}$. The symbols have the same meaning as in Fig. 15.

radiation. Given that harder X-rays will be produced by higher temperature regions it can be seen that the gas between the merging clusters has been heated as it is compressed, similar to our clusters (see panel 1 of Figs 9, 11 and 13).

By the time the subclump reaches R_{500} the cluster will be starting to undergo a merger boost and will start to move up in the L_X–M and T_X–M planes back toward the mean relations. This means that clusters with structure will not necessarily scatter off the T_X–M or L_X–M relations when properties within this radius are considered. Usually the luminosity and temperature increase together pushing the cluster roughly parallel to the L_X–T_X relation. However, if the merger triggers cooling within the cluster core then the X-ray temperature decreases and the cluster will scatter above the L_X–T_X relation and below the T_X–M relation.

As the subclump moves toward the core the compression front will become hotter and closer to the core of both the subclump and the cluster. This means that it will start to ram-pressure strip the subclump of its diffuse ICM. Therefore, even if the core of the subclump survives the merger for a time, the diffuse gas will be assimilated into the cluster by the peak of the merger.

Once the subclump has reached the core, the luminosity and temperature boost will have reached their maximum but, unless the infalling clump has a significant impact parameter, the clus-

ter will be roughly spherical and appear to have little substructure. Grego et al. (2004) observe that the luminous, $z = 0.783$ cluster MS1137.5+6625 appears spherical in the optical and in X-rays but closer inspection with *Chandra* observations show that the cluster is not relaxed. The mass distribution is very compact, consistent with a large amount of recently accreted material. Since the luminosity can be increased at this time by up to an order of magnitude above what a truly relaxed cluster of similar mass would be, then this could impose a bias in a flux-limited sample of clusters, particularly at high redshift, toward clusters at the point of merging.

The effect of merger boosts in biasing the estimate of cluster parameters from high-redshift X-ray cluster observations has been investigated by Randall et al. (2002).

After the peak of the collapse, the core of the subclump will continue to move past or through the core of the cluster. This behaviour has also been observed. *Chandra* observations of 1E0657-56 ($z = 0.296$) presented by Markevitch et al. (2002) observe a 'bullet' which is surmised to be the core of a subcluster. The subcluster has previously passed through the core of the main cluster (approximately 0.1–0.2 Gyr ago) and has had its surrounding gas removed by ram-pressure stripping. It is unclear whether this object exceeds the escape speed of the cluster or not, but it still shows that a subclump can pass through the core of a cluster and that the haloes can merge while the two cores continue on their paths.

If, as is likely, the core of the infalling subclump does not exceed the escape speed, then it will at some later point return to the core and merge. This will cause the luminosity of the core to increase once more. If the temperature profile does not change significantly when this happens, then the increase in emission at the cooler core will cause an emission-weighted temperature for the whole cluster to decrease. This will move the cluster up and to the left on the L_X–T_X plane pushing the cluster above the L_X–T_X relation and so could contribute to the scatter about the relation. By this time the rest of the cluster will have settled down again. This will mean that the luminosity boost at the core will make the core much brighter than the surrounding temperature or luminosity should suggest. This could make the cluster look briefly like a cooling-flow cluster with a very high accretion rate. We find instantaneous mass accretion rates $\dot{M} = L/(5kT/2\mu m_H)$ of up to $700 \, h^{-2} \, {\rm M}_\odot \, {\rm yr}^{-1}$ similar to observed values in high-redshift clusters (Edge et al. 1994; Fabian & Crawford 1995; Allen, Fabian & Kneib 1996; Allen et al. 1996).

The current problem with cooling-flow clusters is that $t_{\rm cool} \ll t_H$ and so a lot of gas should have cooled, but this is not observed (Kaastra et al. 2001; Peterson et al. 2001, 2003). Unfortunately, even considering the Loken, Melott & Miller (1999) result that cooling-flow clusters usually occupy densely populated regions where clusters are more likely to be undergoing mergers, this explanation cannot explain the lack of cold gas in all cooling-flow clusters. A *ROSAT* survey (Peres et al. 1998) found that 70–90 per cent of clusters have cool cores. By their very nature the core mergers are short lived and so would be rare. However, it must be accepted that the accretion of subclumps will continually feed the cores of clusters with low-entropy gas and this must be a contributory factor to the resolution of the cool-core problem. The accretion of low-entropy material by clusters will be investigated in a future paper.

ACKNOWLEDGMENTS

REFERENCES

Allen S.W., Fabian A.C., Edge A.C., Bautz M.W., Furuzawa A., Tawara Y., 1996, MNRAS, 283, 263
Allen S.W., Fabian A.C., Kneib J.P., 1996, MNRAS, 279, 615
Allen S.W., Schmidt R.W., Fabian A.C., 2002, MNRAS, 335, 256
Bond J.R., Efstathiou G.P., 1984, ApJ, 285, L45
Borgani S. et al., 2001, ApJ, 561, 13
Couchman H.M.P., Pearce F.R., Thomas P.A., 1995, MNRAS, 452, 797
Edge A.C., Fabian A.C., Allen S.W., Crawford C.S., White D.A., Böhringer H., Voges W., 1994, MNRAS, 270, L1
Eke V.R., Navarro J.F., Frenk C.S., 1998, ApJ, 503, 569
Fabian A.C., Crawford C.S., 1995, MNRAS, 274, L63
Fairley B.W., Jones L.R., Scharf C., Ebeling H., Perlman E., Horner D., Wegner G., Malkan M., 2000, MNRAS, 315, 669
Grego L., Vrtilek J., Van Speybroeck L., David L.P., Forman W., Carlstrom J.E., Reese E.D., Joy M.K., 2004, ApJ, submitted (astro-ph/0402139)
Holden B.P., Stanford S.A., Squires G.K., Rosati P., Tozzi P., Eisenhardt P., Spinrad H., 2002, AJ, 124, 33
Jenkins A., Frenk C.S., White S.D.M., Colberg J.M., Cole S., Evrard A.E., Couchman H.M.P., Yoshida N., 2001, MNRAS, 321, 372
Kaastra J.S., Ferrigno C., Tamura T., Paerels F.B.S., Peterson J.R., Mittaz J.P.D., 2001, A&A, 365, L99
Lacey C., Cole S., 1993, MNRAS, 262, 627
Lacey C., Cole S., 1994, MNRAS, 271, 676
Loken C., Melott A.L., Miller C.J., 1999, ApJ, 520, L5
Markevitch M., Gonzalez A.H., David L., Vikhlinin A., Murray S., Forman W., Jones C., Tucker W., 2002, ApJ, 567, L27

Maughan B.J., Jones L.R., Ebeling H., Perlman E., Rosati P., Frye C., Mullis C.R., 2003, ApJ, 587, 589
Motl P.M., Burns J.O., Loken C., Norman M.L., Bryan G., 2004, ApJ, 606, 635
Muanwong O., Thomas P.A., Kay S.T., Pearce F.R., 2002, MNRAS, 336, 527
Navarro J.F., Frenk C.S., White S.D.M., 1995, MNRAS, 275, 56
Navarro J.F., Frenk C.S., White S.D.M., 1997, ApJ, 490, 493
Novicki M.C., Sornig M., Henry J.P., 2002, AJ, 124, 2413
Onuora L.I., Kay S.T., Thomas P.A., 2003, MNRAS, 341, 1246
Pearce F.R., Thomas P.A., Couchman H.M.P., 1993, MNRAS, 264, 497
Pearce F.R., Thomas P.A., Couchman H.M.P., 1994, MNRAS, 268, 953
Peres C.B., Fabian A.C., Edge A.C., Allen S.W., Johnstone R.M., White D.A., 1998, MNRAS, 298, 416
Peterson J.R. et al., 2001, A&A, 365, L104
Peterson J.R., Kahn S.M., Paerels F.B.S., Kaastra J.S., Tamura T., Bleeker J.A.M., Ferrigno C., Jernigan J.G., 2003, ApJ, 590, 207
Randall S.W., Sarazin C.L., Ricker P.M., 2002, ApJ, 577, 577
Reiprich T.H., Sarazin C.L., Kempner J.C., 2003, ApJ, submitted (astro-ph/0308282)
Ritchie B.W., Thomas P.A., 2002, MNRAS, 329, 675
Schuecker P., Böhringer H., Reiprich T.H., Feretti L., 2001, A&A, 378, 408
Sutherland R.S., Dopita M.A., 1993, ApJS, 88, 253
Thomas P.A. et al., 1998, MNRAS, 296, 1061
Vikhlinin A., VanSpeybroeck L., Markevitch M., Forman W.R., Grego L., 2002, ApJ, 578, 107
Wechsler R.H., Bullock J.S., Primack J.R., Kravtsov A.V., Dekel A., 2002, ApJ, 568, 52
Zhao D.H., Mo H.J., Jing Y.P., Börner G., 2003, MNRAS, 339, 12

This paper has been typeset from a TeX/LaTeX file prepared by the author.